Available online at www.sciencedirect.com
ScienceDirect
Ore Geology Reviews 32 (2007) 262–274
ORE GEOLOGY REVIEWS
www.elsevier.com/locate/oregeorev

Biogenic and petroleum-related ore-forming processes in Dongsheng uranium deposit, NW China

Chunfang Cai [a,*], Hongtao Li [a], Mingkuan Qin [b], Xiaorong Luo [a], Feiyu Wang [c], Guangxi Ou [b]

[a] *Key Laboratory of Mineral Resources, Institute of Geology and Geophysics, Chinese Academy of Sciences, P.O. Box 9825, Beitucheng Xilu No. 19, Beijing 100029, People's Republic of China*
[b] *Beijing Research Institute of Uranium Geology, Beijing 100029, People's Republic of China*
[c] *Institute of Resource and Information, Petroleum University, Huxue Road, Changping District, Beijing 102249, People's Republic of China*

Received 22 June 2005; accepted 24 May 2006
Available online 21 July 2006

Abstract

Sandstone-hosted roll-type U deposits has recently been found in the Middle Jurassic Zhiluo Formation in the Dongsheng area, north of the Ordos Basin. In order to assess the origin of the uranium mineralization, the host sandstone has been investigated, with emphasis on $\delta^{34}S$ values of ore-stage pyrite, $\delta^{13}C$ of calcite, fluid inclusion oil biomarkers, X-ray diffraction, ICP-MS, as well as studies by electron microprobe and scanning electron microscope. The mineralization consists mainly of coffinite. Some of the coffinite is intimately intergrown with ore-stage pyrite, indicating co-precipitation. Ore-stage pyrite has $\delta^{34}S$ values from −34 to +17‰, suggesting the pyrite sulfur originated from bacterial sulfate reduction. In the host sandstone, calcite cement exhibits $\delta^{13}C$ values from −27.6 to −2.1‰ and fluid inclusion oils show evidence of biodegradation. These lines of evidence indicate petroleum was likely oxidized by sulfate-reducing bacteria (SRB) and thus supplied a source of some of the carbon in the calcite. Microbial degradation of petroleum is partially supported by the low-temperature diagenetic environment (<70 °C). Thus, SRB were likely to reduce sulfates to sulfides simultaneously with petroleum oxidization, and caused direct or indirect reduction of hexavalent uranium [U(VI)] to tetravalent uranium [U(IV)]. U(VI) pre-concentration by adsorption and subsequent inorganic reduction is likely to be less significant than direct reduction of U(VI) by SRB in the Dongsheng deposit. This is because ore-stage solution is non-acidic (pH = 8 to 10), as indicated by abundance of ore-stage pyrite and calcite cement and lack of marcasite in the host sandstone.

Keywords: Bacterial sulfate reduction; Petroleum; $\delta^{13}C$; $\delta^{34}S$; Uranium; Dongsheng; China

1. Introduction

Sandstone-hosted roll-front U deposits were recently discovered in the Yili Basin, the Tuha Basin (Chen et al., 2000) and the Ordos Basin, Northwest China. Now that exploitation of the deposits has begun, they have the potential to become an important source of uranium in China in the future.

Uranium minerals in sandstone-hosted U deposits have frequently been reported to coexist with carbonaceous materials and sulfides. Precipitation of U(VI) has thus been generally considered to result from U

* Corresponding author. Tel.: +86 10 62007375; fax: +86 10 62010846.
E-mail address: cai_cf@yahoo.com (C. Cai).

0169-1368/$ - see front matter © 2006 Elsevier B.V. All rights reserved.
doi:10.1016/j.oregeorev.2006.05.003

(VI) reduction by these materials (e.g., Jensen, 1958; Rackley, 1972; Reynolds and Goldhaber, 1982; Spirakis, 1996). However, several U deposits are located close to oil fields or to uraniferous sandstones containing bitumen or petroleum (e.g., Min et al., 2005a), in which no significant carbonaceous debris has been reported (e.g., Reynolds and Goldhaber, 1982; Milodowski et al., 1990; Landais, 1993; Morrison and Parry, 1998). Only Curiale et al. (1983) have attempted to confirm that petroleum was chemically involved in U(IV) precipitation, although Langmuir (1978) invoked methane as a potential reductant. Reduction of uranium by either sulfides or organic matter is, however, a slow process at low-

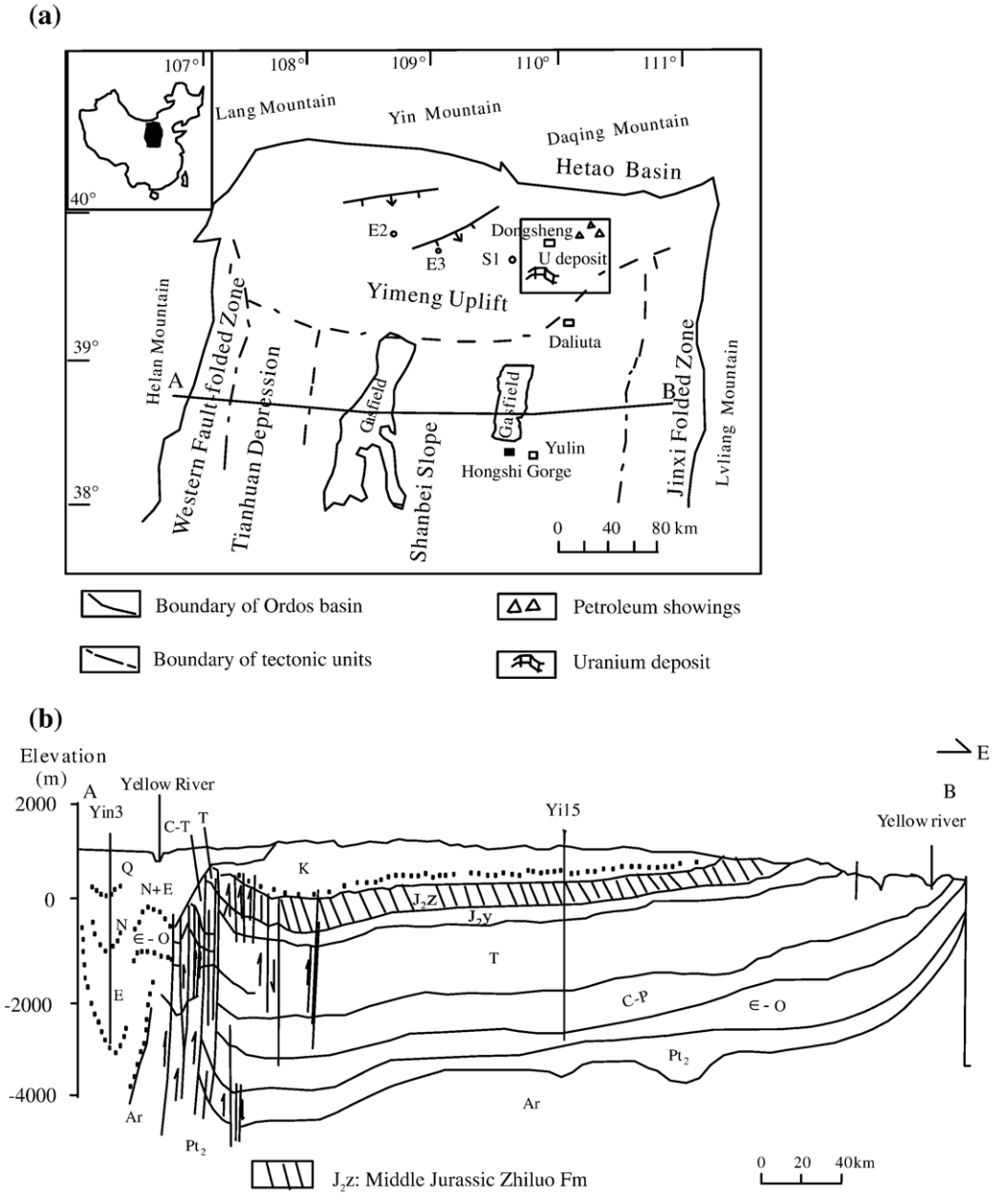

Fig. 1. (a) Map showing the boundary of the Ordos Basin and the location of uranium deposit and petroleum showings. (b) East–West cross-section AB across the north Ordos Basin showing the distribution of Zhiluo Formation (J_2z) sandstone which hosts the Dongsheng deposit.

temperature conditions (Goldhaber et al., 1987) and pre-concentration of U(VI) is required for the reduction and precipitation as U(IV) ore. In contrast, laboratory experiment studies have shown that sulfate-reducing bacteria (SRB) are capable of utilizing U(VI) as the preferred electron acceptor for respiration and reduce U(VI) to U(IV) directly (Lovley and Philips, 1992; Spear et al., 2002; Sani et al., 2004). Thus, the relative importance of enzymatic and inorganic reduction of U (VI) in the U deposit of the Ordos Basin needs to be assessed.

In this contribution, we present sandstone micro-textures, fluid inclusion data, calcite cement $\delta^{13}C$, and pyrite $\delta^{34}S$ data for sandstones hosting deposit in the Dongsheng area of the Ordos Basin. The type of organic matter (kerogen, coal, or petroleum) involved in U(VI) reduction will be addressed along with a hypothesis that enzymatic reduction of U(VI) by microbes is likely to be a more important process for precipitation of uranium ore than adsorption–concentration and inorganic reduction in the deposit.

2. Geological setting

The Dongsheng uranium deposit is located in northern Ordos Basin, northwest China (Fig. 1a). The geology of the Ordos Basin has been reported in Di (2002) and Cai et al. (2005a). Briefly, the basin is bordered to the east by Luliang and Zhongtiao Mountains, to the west by Helan and Liupan Mountains, to the north by Lang, Yin and Daqing Mountains and to the south by Qinling. The basin covers an area of about 370,000 km^2. The basement of the basin is composed of Archean and Lower Proterozoic metamorphic rocks, including granite gneiss, amphibolite, and migmatited granite, and granites of Hercynian-age with relatively high uranium contents. These units form the bedrock exposures in the mountains enclosing the basin (Di, 2002). During the period between the Middle Proterozoic and Paleozoic, the basin was the western part of the North China platform. The Middle and Upper Proterozoic sequence is composed of terrestrial and marine clastics. Paleozoic strata consist of marine carbonates and alternating marine and terrestrial clastic sediments, with

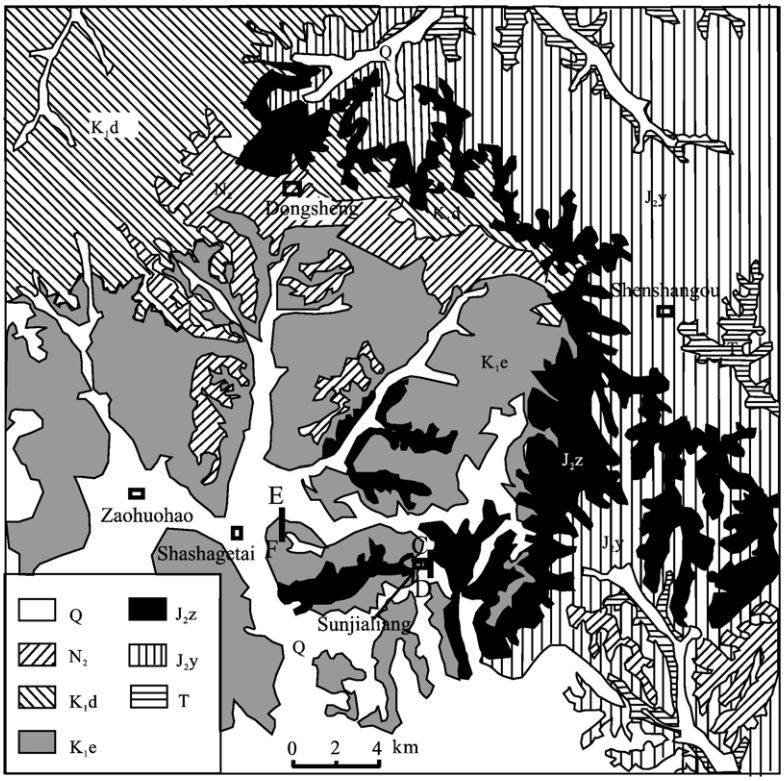

Q: Quaternary
K_1d: Dongsheng Formation of Lower Cretaceous
J_2z: Zhiluo Formation of Middle Jurassic
T: Triassic
N_2: Pliocene
K_1e: Yijinhuoluo Formation of Lower Cretaceous
J_2y: Yanan Formation of Middle Jurassic

Fig. 2. Map showing the geology of Dongsheng area. The location of cross-sections C–D and E–F (Fig. 3) is shown.

interlayered coal beds. Terrestrial sedimentation prevailed since the early Mesozoic. The Triassic–Jurassic sequence is composed of lacustrine and fluvial clastic rocks from which oil and coal are produced. From the end of the Jurassic to the Early Cretaceous, Lvliang Mountain to the east of the basin was uplifted, resulting in the separation of the Ordos Basin from the North China platform, and the formation of a gently westward-sloping monocline (Changqing, 1992) (Fig. 1b). The Lower Cretaceous sequence is composed of up to 1000 m thick sequence of fluvial-facies purplish red mudstone and sandstone containing occurrences of gypsum.

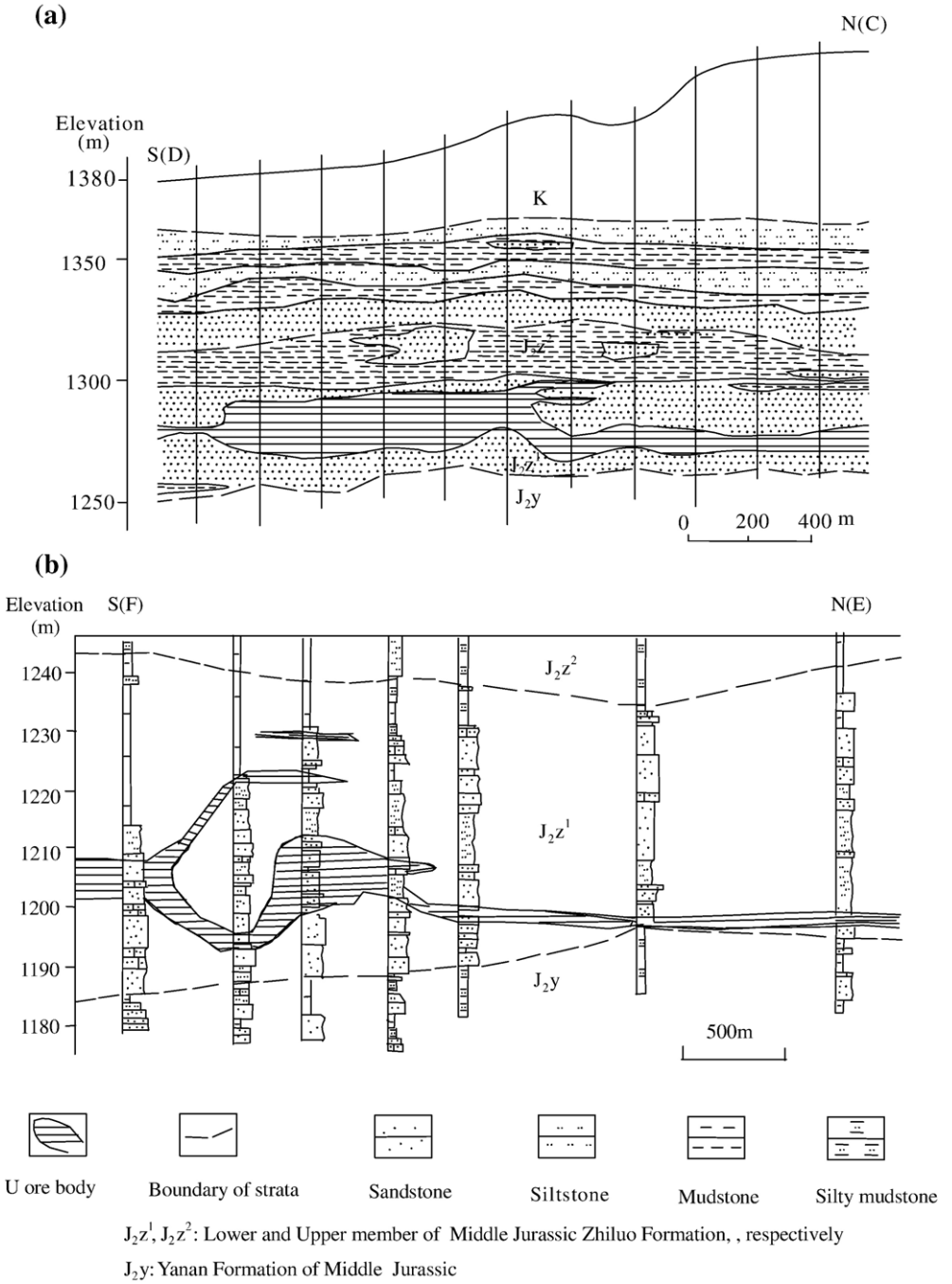

Fig. 3. Cross sections (C–D and E–F), showing uranium orebodies in the Dongsheng deposit: a) tabular to roll-shaped in Sunjialiang sub-deposit and b) roll-shaped in Shashagetai sub-deposit.

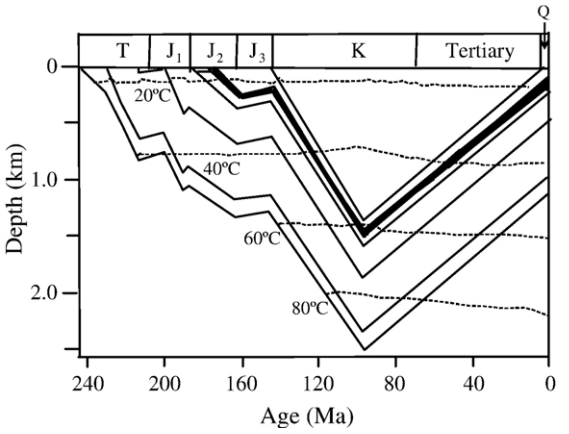

Fig. 4. Burial and thermal history of well S1 modeled on vitrinite reflectance R_o data indicating that Zhiluo Fm (J_2z) experienced a maximum temperature less than 70 °C. See Fig. 1a for location well S1.

Late Yanshanian movement at the end of the Early Cretaceous led to an uplift of the whole basin. Since then, the basin has continually been eroded and the Lower Cretaceous has been exposed at surface in most of the northern Ordos Basin; the structural configuration of the basin has been preserved (Changqing, 1992). As a result, oxidized ground water, which originated by recharge in outcrops toward the north and northwest of the basin, flowed towards the Dongsheng area, supplying uranyl species (and likely sulfates) for the deposit (Chen, 2002).

The Ordos Basin can be divided into six different structural units (Changqing, 1992), including (1) Western fault-folded zone, (2) Tianhuan depression, (3) Shanbei slope, (4) Jinxi folded zone, (5) Weibei uplift and (6) Yimeng uplift. The Yimeng uplift is the area where the Dongsheng uranium deposit is located; this area was uplifted from the Proterozoic to the Late Paleozoic.

3. Geology of the Dongsheng deposit and the host sandstone

The Dongsheng uranium deposit (Fig. 2) includes the Sunjialiang, Zaohuohao, Shashagetai and Daliuta subdeposits. Daliuta is located to the south of the others at longitude 110°15' and latitude 39°16' (Fig. 1a). Oil showings are found in the Lower Cretaceous in outcrop to the northeast of the Dongsheng deposit where the Jurassic to the Middle Triassic has been eroded (Fig. 1a). The sandstone that hosts the U deposit is the Middle Jurassic Zhiluo Formation (Fig. 3). The Zhiluo Formation was deposited in a braided stream to sinuous river environment. It can be divided into the Upper Zhiluo (J_2z^2) and Lower Zhiluo (J_2z^1) members. The Upper member was deposited under a dry to semi-dry climate and is composed of sinuous river facies purplish red, brownish red, or dark purple massive mudstone and sandstone with abundant limonite. The Lower Zhiluo member is the main U-bearing formation (Fig. 3). In the Dongsheng deposit, the host sandstone is composed of braided stream facies grey, grey-green or grey-white middle- to coarse-grained sandstone and contains carbonaceous debris and absorbed petroleum. Away from the roll-front shaped orebodies, for example, in outcrop at Hongshi Gorge to the south of the Dongsheng deposit (Fig. 1a), the Lower Zhiluo member sandstone is brown, brown-red and contains abundant Fe(III)-rich minerals such as limonite and hematite but little carbonaceous debris and pyrite, and no petroleum. It is thus likely that Fe(III) was reduced in the host sandstone in the deposit, perhaps by Fe-reducing bacteria (Lovley et al., 1991).

The host sandstone in the deposit is composed of quartz (40 to 70%), feldspar (15 to 30%) and rock fragments (5 to 25%), and is thus classified as a lithic subarkosic sandstone. The sandstone may contain

Table 1
XRD results (wt.%) of Lower Zhiluo Member (J_2Z^1) host sandstones

No.	Quartz	K-feldspar	Albite	Calcite	Dolomite	Pyrite	Total clay minerals	% of total clay minerals			
								Smectite	Illite	Kaolinite	Chlorite
DS-4	33.6	12.2	8.5	8.5	1.5	tr	35.7	86.0	5	7	2
DS-24	40.9	18.7	13.1	0.7	tr	tr	26.6	57.0	2	21	20
DS-7	27.7	15.7	5.2	0.4	1.6	tr	49.4	64.0	1	14	21
DS-20	41.0	17.0	10.7	tr	2.0	tr	29.3	54.0	2	tr	44
DS-12	26.3	8.8	9.1	24.0	1.4	1.0	19.4	72.0	2	22	4
DS-65	38.4	13.4	12.2	tr	tr	11.1	24.9	77.0	3	10	10
DS-29	43.0	14.0	11.7	3.5	1.0	2.5	24.3	79.0	5	10	6
DS-16	34.3	15.7	11.6	17.5	tr	1.0	19.9	78.0	6	11	5
DS-17	54.4	13.8	8.2	tr	1.7	1.2	20.7	80.0	2	15	3
DS-71	30.6	12.6	9.8	32.2	tr	1.6	13.2	81.0	3	9	7

tr: less than detection limit.

carbonaceous debris but no correlation between uranium content and organic matter has been documented.

The burial and geothermal history of the host sandstone from Well S1 was rebuilt using PRA BasinMod1 software based on vitrinite reflectance R_o values (Ren et al., 2005). Results show that rapid sedimentation took place during the Early to Middle Triassic, in the Middle Jurassic and, finally, in the Cretaceous. Significant uplift occurred during the period from the Late Triassic to Early Jurassic, during the Late Jurassic, and since the end of the Cretaceous (Fig. 4). The host sandstone experienced maximum burial and heating at the end of the Cretaceous and had, at that time, a palaeotemperature of <70 °C (Fig. 4). This is consistent with low R_o values for Jurassic mudstone and coal in the basin in the range from 0.35 to 0.55%.

The Dongsheng uranium deposit consists of tabular to rolled-shaped orebodies (Fig. 3a and b). Individual orebodies extend from several hundred meters up to a kilometer in size in the N–S direction and from several to more than 10 km along the depositional trend or palaeochannel direction. Individual orebodies are generally 3 to 8 m thick, and cumulative thickness reaches up to more than 20 m. The orebodies are mainly low- to medium-grade, typically ranging from 0.03 to 0.5% U_3O_8, although they may locally reach as much as 2.4% U_3O_8. The main uranium mineral is coffinite. The main uranium mineralization near the front of the roll-shaped orebodies has young U–Pb ages, ranging from 20± 2 Ma to 8±1 Ma (Xia et al., 2003), corresponding to the Himalayan orogeny that affected a vast region of NW China. These ages are very similar to those reported for other U deposits in NW China (Min et al., 2005a). On the flanks of the orebodies, the limited available data indicate older U–Pb ages (Xia et al., 2003).

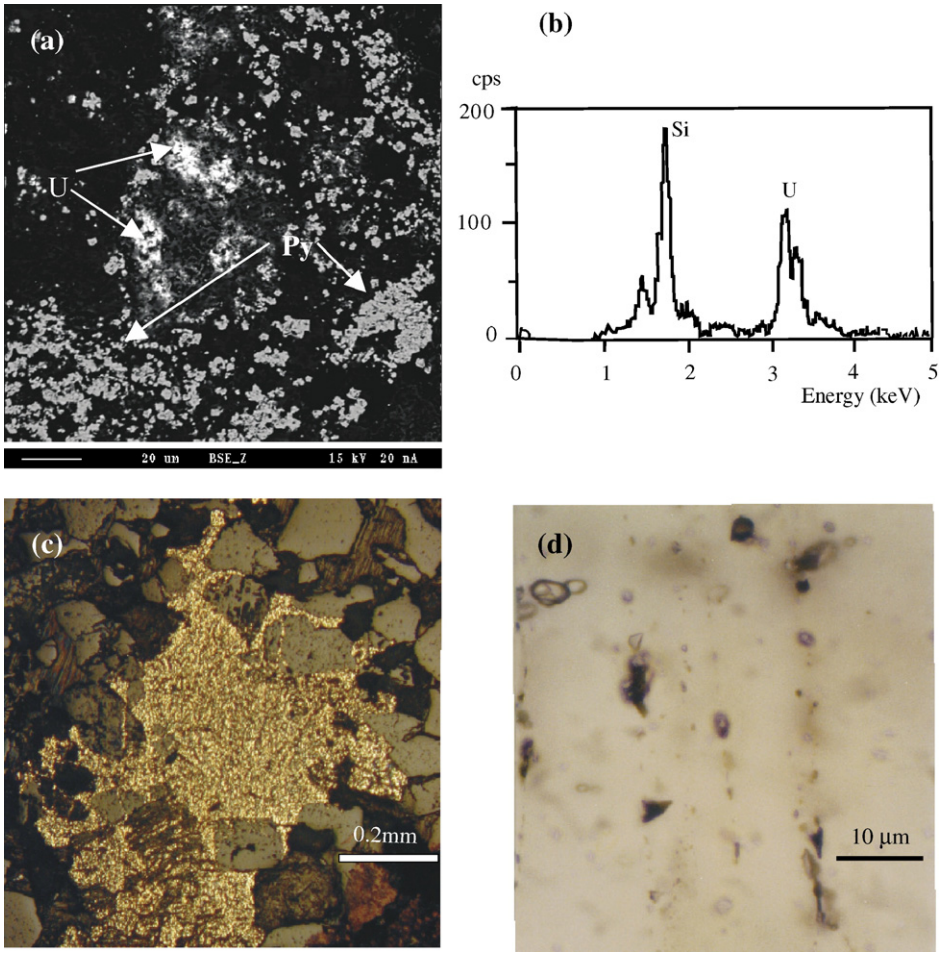

Fig. 5. (a) Microphotograph showing intimate intergrowth of coffinite (U) with secondary pyrite (Py) (back-scatted image, sample No. 26). (b) EDS spectrum from coffinite in (a). Microphotographs showing (c) pyrite aggregates replacing quartz grains, clay matrices and distributing along quartz fractures (reflected light, sample No. 45) (this sample has uranium content of 163.7 µg/g and pyrite $\delta^{34}S$ value of −34‰); (d) secondary oil inclusions in healed quartz microfractures (sample No. 26; transmitted light) (see Table 1 for description of the samples).

4. Sampling and analytical methods

Sandstone samples were collected from the Zhiluo Formation: grey-green sandstone, grey sandstone and mineralized sandstone (Fig. 3a and b). The samples were examined by polarizing microscope, by Shimadzu electron microprobe (EPMA) and D/max 2400 X-ray diffractometer (XRD). Fluid inclusions (FIs) were observed under an ultraviolet fluoroscope. The calcite cement was analyzed for carbon isotopes, and pyrite was handpicked and analyzed for sulfur isotopes. Uranium contents were measured using ICP-MS, with a precision of better than 8%. Results are given in Table 1. Cai et al. (2001) have described the methodologies used for the C and S isotope determinations.

The oil trapped within fluid inclusions in the quartz grains of the sandstones was extracted and analyzed using a method similar to that described by George et al. (2004). Briefly, the sample cuttings were disaggregated, crushed to ~60 mesh, and calcite was dissolved in HCl. Quartz grains were first separated from other minerals, placed in dichloromethane (CH_2Cl_2) solvent for 48 h, and then potential contamination was removed using H_2O_2. Finally, the quartz grains were further crushed to ~200 mesh in solvent (dichloromethane) to release oil from the inclusions into the solvent. The fluid inclusion oils were analyzed using a HP6890 gas chromatography (GC) system. The GC was fitted with a HP5MS 30 m fused silica column (internal diameter 0.25 mm, film thickness 0.25 μm).

5. Results

5.1. Diagenetic minerals and paragenetic sequence

Authigenic minerals in the host sandstone include calcite, dolomite, pyrite, smectite, illite, kaolinite and chlorite cements. No marcasite was detected by XRD analysis and was not observed in polished thin sections. Coffinite is the dominant uranium mineral as confirmed by EPMA. Some of the coffinite is intimately intergrown with secondary pyrite (Fig. 5a and b), suggesting simultaneous precipitation. The paragenetic sequence of the host sandstone is shown in Fig. 6.

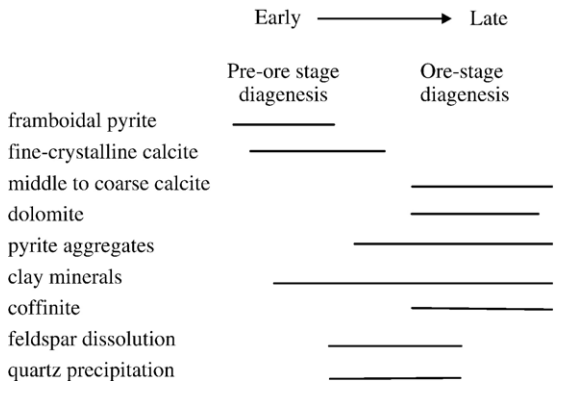

Fig. 6. Proposed paragenetic sequence of the host sandstone (note that ore-stage pyrite is coarsely crystalline or in aggregates, and thus can be handpicked for $\delta^{34}S$ measurement).

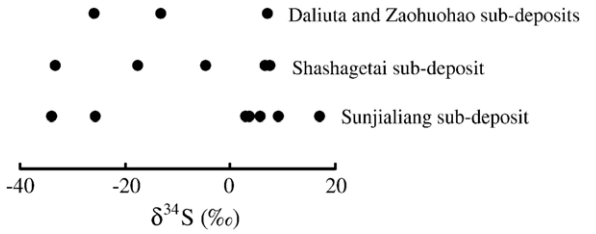

Fig. 7. Ore-stage pyrite $\delta^{34}S$ values showing a wide range from −34‰ to +17‰, indicating origin by bacterial sulfate reduction.

Study of ten samples (Table 1) reveals the following compositions. The compositions are presented in wt.%, as measured by XRD, and in vol.% based on point-counting on thin sections. Pyrite contents of the ore range from 0 to 11.1 wt.%, with an average of 1.8 wt.%. Less than 0.5 vol.% of the pyrite corresponds to pre-ore framboidal type. Ore-stage pyrite occurs as aggregates, which replaced quartz grains and clay matrix, and grows along quartz fractures (Fig. 5c). These features indicate that the pyrite grew at a high crystallization rate under relatively low temperature conditions and postdates the fracturing of quartz. Calcite contents in the sandstone range from 0 to 32.2 wt.%, with an average of 8.7 wt.%. Dolomite contents are <2 wt.%, with an average of 0.9 wt.%. Small amounts of calcite occur as pre-ore calcite characterized by a fine-crystalline texture surrounding detrital grains. Ore-stage calcite occurs as medium- to coarse-crystalline grains in the center of pores, and replaces quartz grains and clay matrix. Authigenic quartz constitutes less than 0.5 vol.% and is typically 5 to 20 μm in size. The quartz cement occurs as pore-filling and is frequently observed to intergrow with chlorite. Feldspar grains have partially been corroded. Dissolution of feldspar may have supplied a source of silicon for coffinite and authigenic quartz. XRD data show that the clay minerals in ten medium- to coarse-grained sandstone samples consist of kaolinite, illite, smectite and chlorite. The contents of total clay minerals in the samples range from 19.4 to 49.4 wt.%. Among the clay minerals, kaolinite has contents from 0 to 22 wt.% (average 11.9 wt.%); illite contents range from 1 to 6 wt.% (average 3.1 wt.%); smectite contents range from 57 to 86 wt.% (average 72.8 wt.%) and chlorite contents range from 2 to 44 wt.%, generally between 5 and 20 wt.%.

Table 2
Uranium contents, calcite cement $\delta^{13}C$ and ore-stage pyrite $\delta^{34}S$ values for Middle Jurassic Zhiluo Formation host sandstones

Deposit	No.	Hole	Depth (m)	Lithology	U (μg/g)	δ^{13}C (‰)	δ^{34}S (‰)
Daliuta	5	SZK2-8	–	grey sandstone	0.84	−15	–
	11	SZK2-3	220.75	grey coarse sandstone	3.57	−27.6	–
	13	SZK2-3	204.7	grey sandstone	–	−12.6	–
	16	SZK2-3	230.75	grey-green sandstone	2.78	−23.5	–
	17	SZK2-3	238	grey-green sandstone	2.29	−20.4	−25.9
Zaohuohao	25	ZKA303	–	grey sandstone	–	–	+7.1
	42−2	ZKA475-115	292	grey sandstone	14.4	−19.7	−13.3
	43	ZKA475-115	–	brown-yellow siltstone	2.9	−18.8	–
Shashagetai	75	ZKA147-39	–	grey-green sandstone	3480.2	−9.7	−17.7
	26	ZKA151-39	166.11	grey coarse sandstone	66.7	−8.8	–
	28	ZKA151-39	167.5	grey coarse sandstone	29.2	−10.6	–
	20	ZKA183-87	153	grey-white siltstone	–	–	+6.7
	22	ZKA183-87	121.43	grey-green siltstone	2.62	–	−33.4
	29	ZKA183-95	–	grey coarse sandstone	6.4	–	+7.5
	30	ZKA183-95	137.28	grey-green sandstone	1.8	−15.9	–
	31−1	ZKA183-95	125.5	grey-green sandstone	2.3	−2.1	–
	32	ZKA183-95	153	grey-green sandstone	30.9	−10.6	−4.7
Sunjialiang	34	ZKA75-51	286.5	grey-green muddy siltstone	4.8	–	+17.0
	35	ZKA75-51	286	grey-white coarse sandstone	0.83	−8.6	−25.6
	37	ZKA75-51	281.5	grey-green fine sandstone	–	–	+9.2
	45	ZK32-60	222.4	grey sandstone	163.6	−12.6	−33.9
	46	ZK32-60	244.65	grey sandstone	6.4	−19.3	+3.0
	49	ZK32-60	135.8	grey muddy siltstone	–	–	+3.6
	50	ZK32-60	140.85	grey calcareous sandstone	0.68	−10.1	+5.6

These clay minerals are mainly authigenic and may have grown during pre-ore and ore-stage diagenesis.

5.2. Isotopic composition of cements

The ore-stage pyrite in the host sandstone from the Dongsheng deposit has $\delta^{34}S$ values ranging from −34 to +17‰ (n=15) (Fig. 7). No correlation is observed between pyrite $\delta^{34}S$ value and whole rock uranium content (Table 2).

Calcite cement has $\delta^{13}C$ values of −2.1‰ to −27.6‰ (n=17), with most of the samples having $\delta^{13}C$ more negative than −10‰ (Table 2), suggesting a significant contribution from organic matter. Some sandstone samples with calcite $\delta^{13}C$ values more negative than −10‰ are shown to have pyrite $\delta^{34}S$ values more negative than −17‰ (Fig. 8), and have high uranium contents (Table 2).

5.3. Analysis of inclusion oils

In the host sandstone, gas and oil inclusions are found to occur in calcite cement as isolated inclusions which appear to be primary and therefore were trapped during crystal growth. Most hydrocarbon inclusions are distributed along healed quartz fractures and thus are secondary (Fig. 5d). The size of the inclusions ranges from 2 to 20 μm, with the majority in the 5 to 10 μm range. Gas inclusions are rich in CH_4 and CO_2. Primary and secondary oil inclusions have the same fluorescence emission color showing light blue to bright white colors, suggesting that both types of inclusions have the similar compositions. The percentage of grains containing oil inclusions in quartz and feldspar grains (GOI; e.g., George et al., 2004) is used as a measure of the extent of oil saturation in the geological past. In the Dongsheng deposit, most samples of the host sandstone have GOI values ranging from 0.2 to 1%. Only a minority of samples have GOI values >5%. The GOI values from 0.2 to 6% in the sandstones indicate that the sandstones may have been utilized as oil migration pathways (e.g., George et al.,

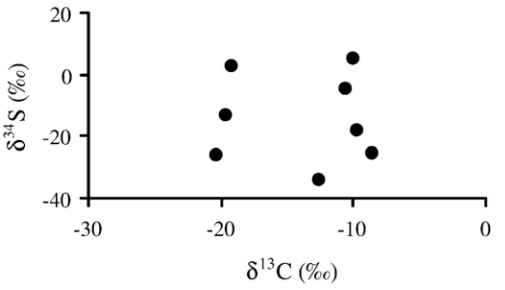

Fig. 8. Plot of calcite $\delta^{13}C$ vs pyrite $\delta^{34}S$ value showing a close association of BSR-derived pyrite with organically derived carbon.

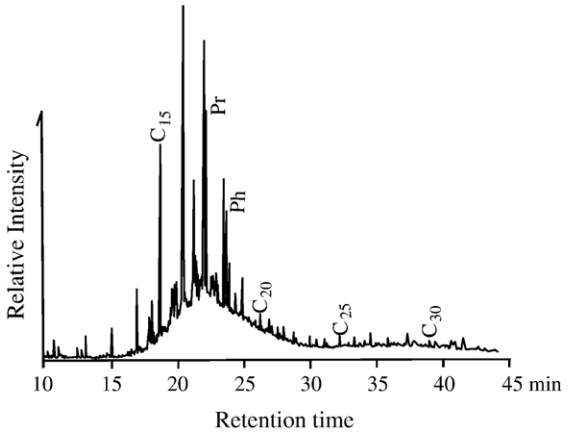

Fig. 9. Gas chromatograph profile showing a hump of unresolved complex mixtures of inclusion oils from Zhiluo Formation sandstone from drillhole ZKA16-32-03 in Shashagetai sub-deposit.

2004), and that oil was most likely escaping during calcite cementation and detrital quartz cracking.

Gas chromatograms (GC) of fluid inclusion oils from the host sandstones show humps of unresolved complex mixtures in the C_{14} to C_{24} carbon number range (Fig. 9). The hump is a prominent feature of analog chromatograms of oils that are depleted in normal and branched alkanes. Pr/n-C_{17} and Ph/n-C_{18} ratios for the inclusion oil from drillhole ZKA7-4-04 sandstone are 0.37 and 0.46, respectively; and they are 0.72 and 0.77 for the inclusion oil from drillhole ZKA16-32-03 sandstone, respectively. Potential source rocks for the fluid inclusion oils include Carboniferous to Permian and Triassic source rocks. In the study, an oil from Triassic source rock shows the same Pr/n-C_{17} and Ph/n-C_{18} ratios of 0.29 whilst a Carboniferous to Permian-derived oil has ratios of <0.2 and <0.4, respectively. The values are significantly lower than those of the fluid inclusion oils in the Dongsheng host sandstone, respectively. The presence of the hump and enrichment in isoprenoids relative to normal alkanes in inclusion oils are the results of biodegradation of the oils (e.g., Jensenius and Burruss, 1990; Cai et al., 1996, 2005b).

6. Discussion

Intimate intergrowth of coffinite with ore-stage pyrite suggests simultaneous co-precipitation, or a genetic link.

6.1. Origin of ore-stage pyrite

The ore-stage pyrite has a $\delta^{34}S$ value as low as −34‰ (Table 2). The value is more negative than the known lightest value of organically derived sulfur [−17‰, see Cai et al. (2002) and references therein], indicating that the reduced sulfur is unlikely to have been derived from organic matter. In addition, no sulfur-rich organic matter was found in petroleum source rocks in the area, indicating that no significant sulfur content was derived from organic matter. This suggests that the sulfur with negative $\delta^{34}S$ values originated by bacterial sulfate reduction (BSR). Sulfate may have been contributed from groundwater and sulfate concentrations are expected to increase when groundwater flowed through Lower Cretaceous gypsum-bearing strata. Another source of sulfate may be from brine which may have migrated upwards along with petroleum. That the pyrite originated via BSR is supported by the low temperature conditions (<70 °C) indicated in the burial-thermal history diagram (Fig. 4), since microbes are generally only active at temperatures <80 °C. The sulfur in pyrite with a $\delta^{34}S$ value down to −34‰ may be a result of multi-step reactions, including sulfate reduction, pyrite oxidation and re-reduction (e.g., Rackley, 1972; Reynolds and Goldhaber, 1982). This is because the maximum achievable fractionation during single-step BSR is −46‰, based on pure culture experiments (Kaplan and Rittenberg, 1964). However, a recent study has shown that the maximum value for single-step fractionation may be as high as −72‰ (Ulrich et al., 2001), although such fractionation is unlikely to be observed in nature.

The high positive $\delta^{34}S$ values of pyrite may be the result of BSR in a relatively closed system. In such a system, the rate of sulfate supply is lower than that of sulfate reduction. As reduction proceeds, newly generated sulfides and residual sulfates are expected to have $\delta^{34}S$ values shifted to positive values (Ohmoto and Rye, 1979).

6.2. Organic matter involved in uranium mineralization

Some studies have suggested that the ubiquitous occurrence of organic matter together with coffinite indicated a genetic link (Hansley and Fitzpartick, 1989; Spirakis, 1996). In the Dongsheng deposit, the host sandstone contains carbonaceous debris, absorbed petroleum and fluid inclusion petroleum. In the following section, we shall discuss which one was chemically involved in uranium mineralization based upon calcite cement $\delta^{13}C$ and molecular biomarker data.

Most of the host sandstone samples have calcite cement $\delta^{13}C$ values that are more negative than −10‰ (Table 2), indicating that part of the carbon is derived from organic matter (OM). Potential OM sources include kerogen from mudstone, *in situ* Jurassic coal and petroleum from deeper strata. OM from mudstone and coal in the Jurassic in the Ordos Basin is dominated by

higher plants and has $\delta^{13}C$ values less negative than −24.0‰ and about −22.4‰, respectively (Chen and Huang, 1997). It seems that the carbon for the calcite with intermediate $\delta^{13}C$ values (Table 2) is derived from Jurassic OM. Wood and Boles (1991) have shown that associated dissolved HCO_3^- would be about 10‰ heavier at 50 °C and about 5‰ heavier at 100 °C than parent OM. Thus, parent OM for the isotopically lightest calcite (−27.6‰) is expected to have $\delta^{13}C$ value of about −33‰, if the whole calcite is generated from oxidization of the OM at about 100 °C. The Jurassic OM $\delta^{13}C$ values are significantly less negative than −27.6‰, and therefore it is unlikely that the carbon, at least for the calcite with the most negative $\delta^{13}C$ values, were derived from Jurassic OM. Instead, the carbon is likely derived from hydrocarbon oxidation, most likely from mixing of CO_2 produced from methane anoxic oxidation with preexisting inorganically derived CO_2 Petroleum was most likely oxidized by microbes in the area, as is evidenced by biodegradation of the inclusion oils (Fig. 9).

There is, however, debate about whether oxic or anoxic bacteria are responsible for the biodegradation of petroleum. Earlier studies show that anoxic sulfate-reducing bacteria are not capable of depleting petroleum directly, but are able to utilize byproducts from hydrocarbon metabolization by oxic bacteria such as organic acids and alcohols (e.g., Jobson et al., 1979; Reynolds and Goldhaber, 1982);

$$2[CH_2O] + SO_4^{2-} = 2HCO_3^- + H_2S$$

in which CH_2O represents organic matter, including functionalized compounds such as carboxylic acids and alcohols.

Furthermore, recent studies have shown that petroleum degradation by anoxic bacteria is very common, although anoxic biodegradation occurs at a slower rate than oxic biodegradation (e.g., Larter et al., 2003). SRB have been shown to utilize long chained alkanes and methane directly or coupled with organic acids (Rueter et al., 1994; Boetius et al., 2000; Cai et al., 2002, 2005b; Zhang et al., 2002) as growth substrates, resulting in the generation of organic CO_2, calcite, H_2S and pyrite as shown in the following equation:

$$SO_4^{2-} + 1.33(-CH_2) + 0.66H_2O \Rightarrow H_2S\uparrow + 1.33CO_2\uparrow + 2OH^-$$

We thus believe that, in the Dongsheng uranium deposit, petroleum was likely depleted by SRB directly. Within and adjacent to the uranium mineralized sandstone, calcite cement associated with biodegraded petroleum in fluid inclusions has $\delta^{13}C$ values mainly from −10.5 to −27.6‰ (Table 1; Fig. 8), suggesting that uranium mineralization and petroleum oxidization are intimately correlated although most of the $\delta^{13}C$ values of calcite can be derived from Jurassic OM.

6.3. Indirect U(VI) reduction by SRB?

Intimate intergrowth and thus simultaneous co-precipitation of coffinite with ore-stage pyrite of BSR origin suggest that coffinite formation is related to BSR. It is generally acknowledged that U(IV) precipitation results from reactions of BSR-derived sulfides (mainly pyrite and H_2S) with uranyl species U(VI) (e.g., Rackley, 1972; Reynolds and Goldhaber, 1982). The reactions are thermodynamically favorable (Langmuir, 1978). However, reduction of uranium by either H_2S or organic matter is a slow process. Some studies (Anderson, 1987; Anderson et al., 1989; Zheng et al., 2002) show that the U(IV) precipitation is not observed to occur in sulfide-containing water columns on modern anoxic marine basins. Experiments by Goldhaber et al. (1987) indicated that H_2S would reduce U at much higher U concentrations than those expected in nature. It is thus necessary for U(VI) to be preconcentrated by adsorption prior to U(VI) reduction. Uranium adsorption is shown to be reversible. Maximum U adsorption occurs in solution with pH values near 6; adsorption is decreased dramatically with an increase in pH values (Goldhaber et al., 1987; Wersin et al., 1994). At pH values above about 7, the uranyl ion forms strong aqueous complexes with carbonate (Grenthe et al., 1992; Langmuir, 1997), inhibiting precipitation or sorption of U (VI). Carbonate and bi-carbonate are common anions in groundwaters (Langmuir, 1997), and are produced by oxidation of organic carbon by bacteria (see above).

Solution pH values can be inferred from diagenetic minerals. Pyrite precipitation and calcite cementation take place at pH about 8 to 10, whereas marcasite precipitation requires a pH of approximately 5 to 6 (Goldhaber et al., 1987). In the Dongsheng deposit, no significant marcasite cement and nor calcite dissolution indicate that the solution during mineralization stage is alkaline. Thus, during the ore-forming stage, U pre-concentration by adsorption and inorganic reduction are unlikely to be significant in this area. Similarly, Zheng et al. (2002) proposed that U(IV) precipitation is probably not by simple inorganic reactions because the accumulation rates of authigenic U precipitated *in situ* do not show a correlation with bottom-water redox conditions in a number of anoxic marine basins.

Inorganic reactions between sulfides and U(VI) may not be a main mechanism for U ore formation in this area. Other mechanisms need to be considered which may account for the formation of coffinite in the Dongsheng deposit.

6.4. U(VI) reduction by SRB directly?

In the Dongsheng area, the majority of pyrite and calcite was precipitated during the ore-forming stage in the host sandstone. The pyrite originated from BSR and part of carbon in the calcite was derived from petroleum (see above). These results and the associated biodegraded hydrocarbons in fluid inclusions, suggest that SRB may have utilized petroleum as a food source, and reduced sulfates to sulfides simultaneously with reduction of U (VI) to insoluble U(IV) ore. This process does not necessitate pre-concentration by adsorption or reduction by sulfides, and has been duplicated by recent laboratory experiments (Lovley and Philips, 1992; Abdelouas et al., 1998; Suzuki et al., 2002; Sani et al., 2004). In contrast, under conditions of low temperatures and without SRB, neither organic matter nor H_2S reacted with U(VI) experimentally (Abdelouas et al., 1998; Sani et al., 2004), probably due to low reaction rates. Milodowski et al. (1990) observed some uranium-mineralized structures related to the activity of filamentous microorganisms in southwest Scotland. In some Chinese sandstone-hosted ore deposit, uranium minerals appear to have psuedomorphically replaced fungi and bacteria (Min et al., 2005b). These lines of evidence indicate that microorganisms play an important role in uranium mineralization. We thus conclude that U(VI) is more likely reduced by SRB directly than by sulfides in the Dongsheng deposit.

6.5. Formation of coffinite

In the Dongsheng area, coffinite is likely to have formed by mixing of brine and petroleum with meteoric water. Meteoric water could have carried uranyl ions and microbes including SRB (e.g., Abdelouas et al., 1998; Cai et al., 2002); whereas petroleum and brine were up-migrated from depths. SRB may have likely degraded petroleum directly, resulting in the generation of organic acids (Cozzarelli et al., 1994; Cai et al., 1996). Subsequently, feldspar dissolved due to the presence of organic acids, supplying a silica source and likely forming organic-silica complexes (Bennett and Siegel, 1987). Partly dissolved feldspar grains and chemically stable organic-silica complexes might provide the high silica activity needed to form coffinite (Brookins, 1976).

7. Conclusions

(1) Coffinite is the main uranium ore mineral in the Middle Jurassic Zhiluo Formation sandstone-hosted deposit of the Dongsheng area.
(2) Coffinite was precipitated simultaneously with pyrite aggregates at temperatures <70 °C.
(3) Bacterial sulfate reduction was responsible for the generation of pyrite aggregates and thus for direct or indirect U(VI) reduction and U(IV) precipitation.
(4) Direct uranium reduction of U(VI) by sulfate reducing bacteria may be more important than inorganic reduction in the deposit.
(5) Sulfate reducing bacteria depleted petroleum from deeper strata rather than terrestrial organic matter *in situ*, resulting in precipitation of calcite with a $\delta^{13}C$ value down to −27.6‰.

Acknowledgements

The research is financially supported by China National Major Basic Development Program "973" (2003CB214605), NSFC (grant No. 40573034) and FANEDD. The authors are grateful to Drs. Vlad Sopuck, Associate Editor Yuanming Pan and Chief Editor Nigel Cook for helpful review and improvement of the English in the manuscript.

References

Abdelouas, A., Lu, Y.M., Lutze, W., Nuttall, H.E., 1998. Reduction of U(VI) to U(IV) by indigenous bacteria in contaminated ground water. Journal of Contaminant Hydrology 35, 217–233.

Anderson, R.F., 1987. Redox behaviors of uranium in an anoxic marine basin. Uranium 3, 145–164.

Anderson, R.F., Fleisher, M.Q., LeHuray, A.P., 1989. Concentration, oxidation state and particulate flux of uranium in the Black Sea. Geochimica et Cosmochimica Acta 53, 2215–2224.

Bennett, P.C., Siegel, D.I., 1987. Increased solubility of quartz in H_2O due to complexing by organic compounds. Nature 326, 684–686.

Boetius, A., Ravenschlag, K., Schubert, C.J., Rickert, D., Widdel, F., Gleseke, A., Amann, R., Jorgensen, B.B., Witte, U., Pfannkuche, O., 2000. A marine microbial consortium apparently mediating anaerobic oxidation of methane. Nature 407, 623–626.

Brookins, D.G., 1976. Position of uraninite and/or coffinite accumulation to the hematite-pyrite interface in sandstone-type deposits. Economic Geology 71, 944–948.

Cai, C.F., Hu, G.Y., He, H., Li, J., Li, J.F., Wu, Y.S., 2005a. Geochemical characteristics and origin of natural gas and thermochemical sulfate reduction in Ordovician carbonates in the Ordos Basin, China. Journal of Petroleum Science and Engineering 48 (3/4), 209–226.

Cai, C.F., Hu, W.S., Worden, R.H., 2001. Thermochemical sulfate reduction in Cambro-Ordovician carbonates in Central Tarim. Marine and Petroleum Geology 18, 729–741.

Cai, C.F., Mei, B., Ma, T., Chen, C., Liu, C., 1996. Hydrocarbons-water-rock interaction in the diagenetically altered system nearby the unconformities. Chinese Sciences Bulletin 41, 1631–1635.

Cai, C.F., Worden, R.H., Wang, Q.H., Xiang, T.S., Zhu, J.Q., Chu, X.L., 2002. Chemical and isotopic evidence for secondary alteration of natural gases in the Hetianhe Field, Bachu Uplift of the Tarim Basin. Organic Geochemistry 33, 1415–1427.

Cai, C.F., Worden, R.H., Wolff, G.A., Bottrell, S., Wang, D.L., Li, X., 2005b. Origin of sulfur rich oils and H_2S in Tertiary lacustrine sections of the Jinxian Sag, Bohai Bay Basin, China. Applied Geochemistry 20, 1427–1444.

Changqing (Petroleum Geology Group of Changqing Oilfield), 1992. Petroleum Geology of China volume 12: Changqing Oilfield. Petroleum Industry Press, Beijing, pp. 62–78 (in Chinese).

Chen, F.Z., 2002. Analysis on palaeohydrogeological conditions and prospects of uranium metallogenesis in northern part of Ordos basin. Uranium Geology 20, 141–145 (in Chinese).

Chen, J.P., Huang, D.F., 1997. The source of oils in Jurassic coal mine in the southeast of Ordos basin. Acta Sedimentologica Sinica 15 (2), 100–104 (in Chinese).

Chen, Z.B., Zhao, F.M., Xiang, W.D., Chen, Y.H., 2000. Uranium provinces in China. Acta Geologica Sinica 74, 587–594.

Cozzarelli, H.M., Jo Baedecker, M., Eganhouse, R.P., 1994. The geochemical evolution of low-molecular-weight organic acids derived from the degradation of petroleum contamination in groundwater. Geochimica et Cosmochimica Acta 58, 863–877.

Curiale, J.A., Bloch, S., Rafalska-Bloch, J., Harrison, W.E., 1983. Petroleum-related origin for uraniferous organic-rich nodules of southwestern Oklahoma. American Association of Petroleum Geologists Bulletin 67, 588–608.

Di, Y.Q., 2002. Preliminary discussion of prospecting potential for sandstone-type uranium deposits Meso–Cenozoic basins, northern Ordos. Uranium Geology 18, 340–347 (in Chinese).

George, S.C., Ahmed, M., Liu, K., Volk, H., 2004. The analysis of oil trapped during secondary migration. Organic Geochemistry 35, 1489–1511.

Goldhaber, M.B., Hemingway, B.S., Mobagheghi, A., Reynolds, R.L., Northrop, H.R., 1987. Origin of coffinite in sedimentary rocks by a sequential adsorption–reduction mechanism. Bulletin of Mineralogy 110, 131–144.

Grenthe, I., Fuger, J., Konings, R.J.M., Lemire, R.J., Muller, A.B., Nguyen-Trung, C., Wanner, H., 1992. Chemical thermodynamics. Vol. 1: Chemical thermodynamics of uranium. OECE-NEA Elsevier.

Hansley, P.L., Fitzpartick, J.J., 1989. Compositional and crystallographic data on REE-bearing coffinite from the Grants uranium region, northwestern New Mexico. American Mineralogist 74, 263–270.

Jensen, M.L., 1958. Sulfur isotopes and the origin of sandstone-type uranium ore deposits. Economic Geology 53, 598–616.

Jensenius, J., Burruss, R.C., 1990. Hydrocarbon-water interactions during brine migration: evidence from hydrocarbon inclusions in calcite cements from Danish North Sea oil fields. Geochimica et Cosmochimica Acta 54, 705–713.

Jobson, A.M., Cook, F.D., Westlake, D.W.S., 1979. Interaction of aerobic and anaerobic bacteria in petroleum biodegradation. Chemical Geology 24, 355–465.

Kaplan, I.R., Rittenberg, S.C., 1964. Microbiological fractionation of sulfur isotopes. Journal of General Microbiology 34, 195–212.

Landais, P., 1993. Bitumens in Uranium Deposits. In: Parnell, J., Kucha, H., Landais, P. (Eds.), Bitumens in Ore Deposits. Springer-Verlag, Berlin, pp. 213–238.

Langmuir, D., 1978. Uranium solution-mineral equilibria at low temperature with applications to sedimentary ore deposits. Geochimica et Cosmochimica Acta 42, 547–569.

Langmuir, D., 1997. Aqueous Environmental Geochemistry. Prentice-Hall, Engelwood Cliffs New Jersey. 600 pp.

Larter, S., Wilhelms, A., Head, I., Koopmans, M., Aplin, A., Di Primio, R., Zwach, C., Erdmann, M., Telnaes, N., 2003. The controls on the composition of biodegraded oils in the deep subsurface — part 1: biodegradation rates in petroleum reservoirs. Organic Geochemistry 34, 601–613.

Lovley, D.R., Philips, E.J.P., 1992. Reduction of uranium by Desulfovibrio desufuricans. Applied Environment Microbiology 58, 850–856.

Lovley, D.R., Philips, E.J.P., Gorby, Y.A., Landa, E.R., 1991. Microbial reduction of uranium. Nature 350, 413–416.

Milodowski, A.E., West, J.M., Pearce, J.M., Hyslop, E.K., Basham, I.R., Hooker, P.J., 1990. Uranium-mineralized microorganisms associated with uraniferous hydrocarbons in southwest Scotland. Nature 347, 465–467.

Min, M.Z., Chen, J., Wang, J.P., Wei, G.H., Fayek, M., 2005a. Mineral paragenesis and textures associated with sandstone-hosted roll-front uranium deposits, NW China. Ore Geology Reviews 26, 51–69.

Min, M.Z., Xu, M.H., Chen, J., Fayek, M., 2005b. Evidence of uranium biomineralization in sandstone-hosted roll-front uranium deposits, northwestern China. Ore Geology Reviews 26, 198–206.

Morrison, S.J., Parry, W.T., 1998. Age and formation conditions of alteration associated with a collapse structure, Temple Mountain uranium district, Utah. Geological Society of America Bulletin 100, 1069–1077.

Ohmoto, H., Rye, R.O., 1979. Isotopes of sulfur and carbon. In: Barnes, H.S. (Ed.), 2nd ed. Geochemistry of Hydrothermal Ore Deposits. Wiley Interscience, New York, pp. 509–567.

Rackley, R.I., 1972. Environment of Wyoming Tertiary uranium deposits. American Association of Petroleum Geologists Bulletin 56, 755–774.

Ren, Z.L., Zhang, S., Gao, S.L., Cui, J.P., 2005. Present situation and progress on thermal history research of Ordos basin. In: Liu, C.Y. (Ed.), Advances in the accumulation and formation for multi-energy mineral deposits coexisting in the same basin. Science Press, Beijingp, pp. 17–25 (in Chinese).

Reynolds, R.L., Goldhaber, M.B., 1982. Biogenic and nonbiogenic ore-forming processes in the South Texas uranium district: evidence from the Panna Maria deposit. Economic Geology 77, 541–556.

Rueter, P., Rabus, R., Wilkes, H., Aeckersberg, F., Rainey, F.A., Jannasch, H.W., Widdel, F., 1994. Anaerobic oxidation of hydrocarbons in crude oil by new types of sulfate-reducing bacteria. Nature 372, 455–458.

Sani, R.K., Peyton, B.M., Amonette, J.E., Geesey, G.G., 2004. Reduction of uranium(VI) under sulfate-reducing conditions in the presence of Fe(III)-(hydr)oxides. Geochimica et Cosmochimica Acta 68, 2639–2648.

Spear, J.R., Figueroa, L.A., Honeyman, B.D., 2002. Modeling the removal of uranium U(VI) from aqueous solutions in the presence of sulfate reducing bacteria. Applied Microbiology and Biotechnology 60, 192–199.

Spirakis, C.S., 1996. The roles of organic matter in the formation of uranium deposits in sedimentary rocks. Ore Geology Reviews 11, 53–69.

Suzuki, Y., Kelly, S.D., Kenneth, M.K., Banfield, J.F., 2002. Radionuclide contamination: nanometer-size products of uranium bioreduction. Nature 419, 134–136.

Ulrich, G.W., Stefano, M.B., Michael, E.B., 2001. Hypersulfidic deep biosphere indicates extreme sulfur isotope fractionation during single-step microbial sulfate reduction. Geology 29, 647–650.

Wersin, P., Hochella Jr, M.F., Persson, P., Redden, G., Leckie, J.O., Harris, D.W., 1994. Interaction between aqueous uranium (VI) and

sulfide minerals: spectroscopic evidence for sorption and reduction. Geochimica et Cosmochimica Acta 58, 2829–2843.

Wood, J.R., Boles, J.R., 1991. Evidence for episodic cementation and diagenetic recording of seismic pumping events, North Coles Levee, California U.S.A. Applied Geochemistry 6, 509–521.

Xia, Y.L., Lin, J.R., Liu, H.B., Fan, G., Hou, Y., 2003. Research on geochronology and sandstone-hosted uranium ore formation in major uranium productive basins, northern China. Uranium Geology 19 (3), 129–136 (in Chinese).

Zhang, C.L., Li, Y.L., Wall, J.D., Larsen, L., Sassen, R., Huang, Y.S., Wang, Y., Peacock, A., White, D.C., Horita, J., Cole, D.R., 2002. Lipid and carbon isotopic evidence of methane-oxidizing and sulfate-reducing bacteria in association with gas hydrates from the Gulf of Mexico. Geology 30, 239–242.

Zheng, Y., Anderson, R.F., van Geen, A., Fleisher, A.Q., 2002. Remobilization of authigenic uranium in marine sediments by bioturbation. Geochimica et Cosmochimica Acta 66, 1759–1772.